


Article

Influence of Supercritical CO₂ Fluid on CH₄ and CO₂ Diffusion in Vitrinite-Rich Coals and Inertinite-Rich Coals

Wei Li ^{1,2,*}, Weili Lin ³, Hongfu Liu ⁴, Xiaoxia Song ⁴  and Zhenji Wei ⁵

¹ Key Laboratory of Continental Shale Hydrocarbon Accumulation and Efficient Development of Ministry of Education, Northeast Petroleum University, Daqing 163318, China

² Institute of Unconventional Oil & Gas, Northeast Petroleum University, Daqing 163318, China

³ School of Earth Sciences, Northeast Petroleum University, Daqing 163318, China

⁴ Department of Earth Science and Engineering, Taiyuan University of Technology, Taiyuan 030024, China

⁵ China United Coalbed Methane National Engineering Research Center Co., Ltd., Beijing 100095, China

* Correspondence: pingyaoliwei@nepu.edu.cn

Abstract: Coal maceral composition has a great effect on gas adsorption and diffusion. The interaction between maceral composition and supercritical CO₂ (SCCO₂) fluid will affect gas diffusion behavior in coals. Thus, the diffusivity derived from adsorption kinetics of CH₄ and CO₂ in vitrinite- and inertinite-rich coals with low-volatile bituminous rank collected from the Hancheng mine of the Weibei coalfield pre- and post-SCCO₂ fluid exposure (SFE) were tested at the conditions of 45 °C and 0.9 MPa. In combination with pore distribution and functional group content, the possible mechanism of the alterations in gas diffusion characteristics in coals with various maceral compositions was addressed. The results show that for vitrinite-rich coals, SFE increases the macropore apparent diffusion coefficient of CH₄, while this treatment decreases the micropore apparent diffusion coefficient of CH₄. However, the reverse trend is found for CO₂ diffusion-adsorption rate. For inertinite-rich coals post-SFE, CH₄ diffusion-adsorption rate increases, while an increase and a decrease in diffusivity CO₂ occur for macropore and micropore, respectively. Generally, SFE shows a stronger impact on CO₂ adsorption rate than CH₄ in coals. The results suggest that the diffusion of CH₄ and CO₂ in coals with different maceral compositions show selectivity to SCCO₂ fluid. The possible reason can be attributed to the changes in pore structure and surface functional group content. SFE causes an increase in macro/mesopore volume of all samples. However, SFE induces a reduction in oxygen-containing species content and micropore volume of inertinite-rich coals, while the opposite trend occurs in vitrinite-rich coals. Thus, the changes in pore volume and surface functional group account for the difference in gas diffusivity of coals with different maceral compositions. With regard to the micropore diffusion-adsorption behavior of CH₄ and CO₂, the impact of oxygen-containing species is superior to pore volume. The oxygen-containing species favor CO₂ diffusion-adsorption but go against CH₄ transport. This effect accounts for the reduction in the micropore diffusion-adsorption rate of CH₄ and the increase in micropore diffusivity of CO₂ in vitrinite-rich coals, respectively. However, the aforementioned effect is the opposite for inertinite-rich coals. Overall, the changes in gas diffusion in coals with different maceral composition during the CO₂-ECBM process requires further attention.

Keywords: supercritical fluid; CO₂ sequestration; maceral composition; adsorption; diffusion



Citation: Li, W.; Lin, W.; Liu, H.; Song, X.; Wei, Z. Influence of Supercritical CO₂ Fluid on CH₄ and CO₂ Diffusion in Vitrinite-Rich Coals and Inertinite-Rich Coals. *Energies* **2023**, *16*, 1432. <https://doi.org/10.3390/en16031432>

Academic Editors: Yong Li, Fan Cui, Chao Xu and Liu Yang

Received: 11 December 2022

Revised: 24 January 2023

Accepted: 30 January 2023

Published: 1 February 2023



Copyright: © 2023 by the authors. Licensee MDPI, Basel, Switzerland. This article is an open access article distributed under the terms and conditions of the Creative Commons Attribution (CC BY) license (<https://creativecommons.org/licenses/by/4.0/>).

1. Introduction

The emission of carbon dioxide (CO₂) has led to serious global warming, which has brought a series of global environmental issues [1]. Multiple research has confirmed that the geo-sequestration of CO₂ in coal seams has become a potential technology to mitigate CO₂ emissions and to enhance CH₄ production (CO₂-ECBM) [2–4], which can store CO₂ in geologic time [5,6]. Most investigations suggest that the depth of CO₂ sequestration in coal seams is always above 800 m [6], in which the reservoir conditions exceed the critical points

of CO₂ (31.05 °C and 7.38 MPa). As a result, as can be seen in Figure 1, CO₂ is presented as supercritical CO₂ fluid (SCCO₂) [7]. In this situation, the thermophysical properties of CO₂ (viscosity, density, surface tension, etc.) undergo a great change [8–10]. SCCO₂ with low viscosity, low surface tension, and high density can extract hydrocarbons from the coal matrix [11]. The extraction effect and complex SCCO₂-coal interaction can alter the physical and chemical characteristics of coals [12,13].

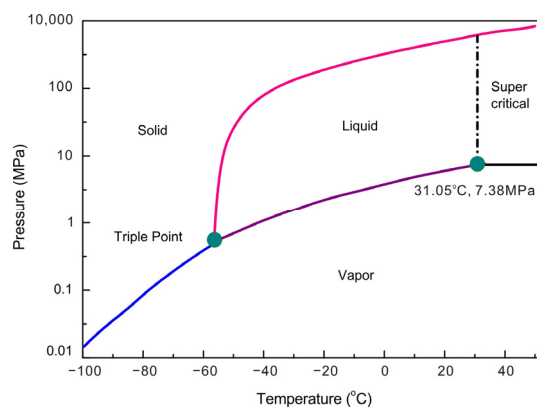


Figure 1. Phase state of CO₂ with varying temperature and pressure (modified from Holliday et al. [7]).

Sampath et al. [14] investigated the changes in coal pore parameters after different interaction time of SCCO₂ with coal, and the results indicated that the reduction in pore parameters occurred after hours of SCCO₂ treatment, but the increases were recorded after weeks of SCCO₂ interaction. They concluded that the different alterations in pore structure at a given SCCO₂ time were related to the comprehensive effects of multiple processes. Chen et al. [15] investigated the influence of SCCO₂ on nanopore distribution of various rank coals at conditions of 12 MPa and 323.15 K. During SCCO₂ for 10 days, they found that the micropore volume decreased but the macropore volume obviously increased. Additionally, the impact of SCCO₂ showed selectivity to coal rank. Gao et al. [16] examined the change in the pore structure of anthracite coals after the CO₂-H₂O reaction at conditions of 5 MPa and 40 °C. The results revealed that the mineral compositions played an important role in the alterations in pore shape, pore type, pore volume, and connectivity. They suggested that the interaction of CO₂-H₂O with anthracite benefited pore modification. The work of Zhang et al. [17] investigated the change in the chemical structure of coals after SCCO₂ treatment by synchrotron ATR-FTIR microspectroscopy. The results showed that the aromaticity of high-volatile bituminous coal and low-volatile bituminous coal increased by different degrees owing to the loss of alkanes. Their findings provided further evidence of SCCO₂ extraction and reinforced the concept of plasticization of coal after SCCO₂ exposure. In recent work, Zhang et al. [18] studied the responses of microstructures and nanoscale mechanical properties of anthracite coal to SCCO₂ by using optical microscopy and nanoindentation. The results of nanoindentation directly testified to the softening effects of SCCO₂ by the changes in Young's modulus and hardness. Overall, the CO₂ adsorption capacity of coals changed owing to the alterations in physical and chemical structure [19–22].

Hitherto, the change in coal structure and CO₂ adsorption capacity due to SCCO₂-coal interaction is related to coal maceral composition and coal type [23,24]. Mastalerz et al. [25] investigated the change in pore distribution of vitrain, clarain, and fusain lithotypes after exposure to gaseous CO₂. They found that the pore structure of clarain after gaseous CO₂ exposure showed minor change, while the changing trend in pore properties of vitrain and fusain was the opposite. Cao et al. [26] analyzed the interaction between the chemical structure of coal lithotypes and gaseous CO₂. They found that a decline in aromaticity and an increase in aliphatic carbons occurred in vitrain and fusain after CO₂ adsorption, whereas reverse results were found in clarain and bright clarain. Karacan et al. [27] found that vitrinite exhibited matrix swelling after CO₂ adsorption, while inertinite showed

matrix compression. Maphala and Wagner [28] studied the interaction between sub-critical CO₂ and maceral composition of high-volatile bituminous coals. The results demonstrated that no significant difference in pore structure was observed for inertinite-rich coals after CO₂ exposure, while obvious alteration was found for vitrinite-rich coals. Nevertheless, the CO₂ adsorption amounts of both inertinite- and vitrinite-rich coals increased after exposure to CO₂. Mavhengere et al. [29] investigated the interactions of sub-critical CO₂ and SCCO₂ fluid with medium bituminous coals. They concluded that the changes in pore properties and chemical structure of vitrinite-rich coals and inertinite-rich coals are different. However, SCCO₂ fluid improved CO₂ adsorption capacity of all samples.

In summary, SCCO₂ fluid exposure (SFE) alters the physicochemical properties of coals with various maceral compositions. Notwithstanding, the alterations in diffusivity of CH₄ and CO₂ in coals are also important to CO₂-ECBM [30,31]. The diffusion-adsorption rate or diffusivity of CH₄ and CO₂ is crucial to the CO₂ injection rate and CH₄ recovery efficiency during the implementation of the CO₂ sequestration process [32–35]. Keshavarz et al. [36] reported the influence of maceral composition on the CH₄ and CO₂ diffusivity of bituminous and sub-bituminous coals. They found that the gas diffusion rate increased with the increasing inertinite content. The work of Guang et al. [37] showed that CO₂ pressure had a critical effect on gas diffusivity in sub-bituminous coals. Goodman et al. [38] studied the effect of gaseous CO₂ on CO₂ diffusion in high-volatile bituminous coals at low pressure (<0.62 MPa). Wang et al. [39] studied the diffusivity of CO₂ and CH₄ in high-volatile bituminous coals and anthracite pre- and post-SCCO₂ exposure. However, little attention is paid to the role of maceral composition in the influence of SCCO₂ fluid on CH₄ and CO₂ diffusion in low-volatile bituminous coals. Thus, as for low-volatile bituminous coals, the present study aims to analyze the influence of SFE on CH₄ and CO₂ diffusivity in vitrinite- and inertinite-rich coals. Moreover, the mechanisms of SFE dependence on gas diffusion are addressed.

2. Materials and Methods

2.1. Characteristics of Coal Samples

All the studied samples were obtained from the Hancheng coalmine of the Webei coalfield located in the southeastern margin of Ordos Basin. The detailed geological setting of the selected coal samples has been described in our previous work [40]. Among the samples, XS9 and XS1 samples were collected from the XS coal mine, and SSP17 and SSP16 samples were from the SSP coal mine (Table 1). According to GB/T 6948-2008 and GB/T 8899-2013 standards, the maximum vitrinite reflectance ($R_{o,max}$) and maceral composition content were measured, respectively. Based on the GB/T 212-2008 standard, the proximate analysis (moisture, ash, and volatile) of samples (air dried basis) is given in Table 1. The values of $R_{o,max}$ and volatile matter yield indicate that all the samples belonged to low-volatile bituminous coals. Based on an arbitrary 50% inertinite boundary, as suggested by Unsworth et al. [41], vitrinite-rich coals and inertinite-rich coals could be identified. Thus, XS9 and XS1 samples were classified into vitrinite-rich coals, while SSP17 and SSP16 samples were inertinite-rich coals.

Table 1. Information of coal samples including $R_{o,max}$, maceral composition, and proximate analysis.

Sample Number	$R_{o,max}$ (%)	Maceral Composition (vol, %)			Proximate Analysis (wt, %)		
		Vitrinite	Inertinite	Minerals	Moisture	Ash	Volatile
XS9	1.777	83.7	15.7	0.6	0.70	12.82	14.59
XS1	1.720	80.9	18.2	0.9	0.66	13.97	14.73
SSP17	1.745	12.3	87.3	0.4	1.00	6.88	15.14
SSP16	1.797	19.5	79.5	1.0	0.89	11.19	16.18

2.2. Geochemical Interaction of SCCO₂ Fluid with Coal Samples

A supercritical fluid interaction apparatus (Thar Process, Inc., Pittsburgh, PA, USA), shown in Figure 2, was employed to conduct the geochemical interaction of SCCO₂ fluid with drying coal samples. The detailed apparatus information can be found in our previous work [42]. During the SCCO₂-coal interaction, a long duration may be needed to achieve the SCCO₂ equilibrium state for large particle sizes due to the long migration path [43,44], which may result in slow interaction efficiency between SCCO₂ and coal. As suggested by Goodman et al. [38] and Wang et al. [39], in order to enhance the interaction efficiency, 80–120 mesh particle samples were sieved to conduct the experiment. Prior to the interaction measurement, the samples were put into a vacuum drying oven to remove moisture. The drying temperature and time were 105 °C and 24 h, respectively. Subsequently, 50 g of particle samples were moved into the interaction/extraction vessel to conduct the geochemical interaction of SCCO₂ fluid with particle samples. The interaction temperature of 45 °C and pressure of 12 MPa were chosen as simulative reservoir conditions with a depth of 1200 m for geologic sequestration of CO₂. The mass flow rate and exposure duration of SCCO₂ fluid were set as 10 g/min and 12 h, respectively, according to previous works [39,45]. At the end of the exposure, all the samples were degassed in a vacuum drying oven at 105 °C for 24 h. Finally, all the samples were stored in a closed cell filled with inert helium prior to subsequent characterizations and measurements.

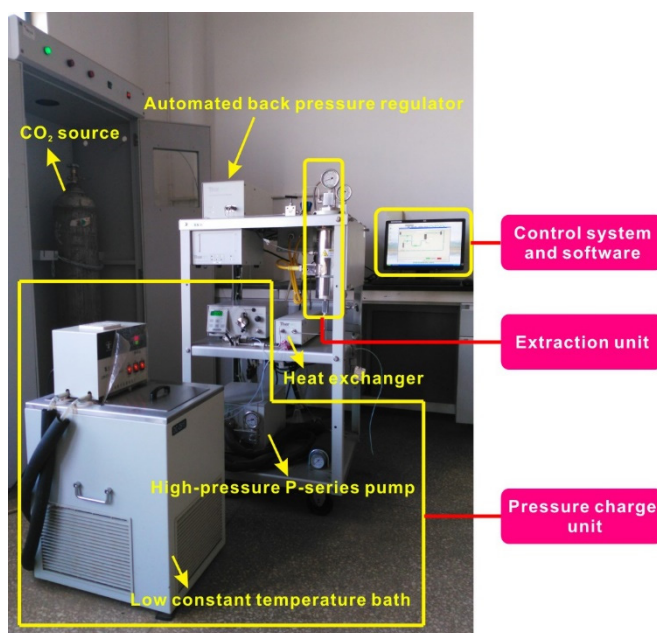


Figure 2. Dynamic supercritical fluid geochemical interaction apparatus.

2.3. Pore Volume and Specific Surface Area Analysis

The pore volume (PV) and specific surface area (SSA) were measured by ASAP2460 adsorption apparatus (Micromeritics, Norcross, GA, USA). The remaining moisture and gas in samples pre- and post-SFE were removed by drying at 105 °C for 24 h before pore analysis. N₂ and CO₂ were selected as a molecular probe to detect macro/mesopore parameters and micropore parameters at 77 K and 273 K, respectively. The PV and SSA of macro/mesopores were determined by BET and BJH model, respectively. Both the PV and SSA of micropores were obtained by the DR model. The corresponding pore diameter range for macro-, meso- and micropores were divided into >50 nm, 2–50 nm, and <2 nm, as suggested by the work of Sing et al. [46].

2.4. X-ray Photoelectron Spectroscopy Measurement

The X-ray photoelectron spectroscopy (XPS) analysis of all samples was measured by PHI 5000 VersaProbe-II spectrometer. The surface element content including C1(s), O1(s),

N1(s), S2(p), C1(s), Al2(p), Si2(p) was obtained with 36 scans. The test was performed at 200 W and 15 kV. The charge correction of the surface element was conducted based on the C1(s) peak at 284.8 eV. According to the work of Weitzsacker et al. [47], the inorganic O derived from SiO₂ and AlO_{1.5} had a great effect on the distribution of organic O in coals. Thus, in order to obtain the organic O content in coals, the inorganic O concentration was subtracted from the total surface O1(s).

2.5. Diffusion–Adsorption Measurement

The diffusion–adsorption test of CH₄ and CO₂ in coals pre- and post-SFE was carried out using a volumetric technique through high-pressure isothermal adsorption apparatus. The detailed parameters of the experimental rig can be found in our previous work [42]. Before the test, all the samples were put into a vacuum drying oven to remove moisture at 105 °C for 24 h. Each sample with a mass of 40 ± 0.0005 g was used for gas diffusion–adsorption test. The experimental temperature of 45 °C and pressure of 0.9 MPa were selected to perform for CH₄ and CO₂ adsorption. Particularly, the recording frequency of pressure data was set as 1 s.

According to the principle of mass conservation, the time-based testing data of the adsorption amount can be calculated by:

$$\Delta\text{GSE} = \frac{1}{RmT} \left(\frac{P_2 V_{\text{RC}}}{Z_2} + \frac{P_1 V_V}{Z_1} - \frac{P_3 V_{\text{RC}}}{Z_3} - \frac{P_4 V_V}{Z_4} \right) \quad (1)$$

where GSE is the experimentally observed Gibbrian surface excess amount, mmol/g; R is the universal gas constant, 8.314 J/mol/K; m is the mass of samples, g; T is the testing temperature, K; V_{RC} and V_V is the volume of the reference and adsorption cell, respectively, m³; P_1 and P_2 are the initial pressures of sample cell and a reference cell, respectively, MPa; P_3 and P_4 are the instantaneous pressures of the reference cell and adsorption at time of t , respectively, MPa; Z are the compressibility factors of CH₄ or CO₂. In this study, the compressibility factors of CH₄ and CO₂ were calculated by Wagner and Span-EOS [48] and Span and Wagner-EOS with high predictive accuracy [49], respectively. Based on the data log of pressure against t , the CH₄ and CO₂ adsorption capacity at a given t were obtained through Equation (1), followed by the CH₄ or CO₂ adsorption rate curves. It should be noted that the calculation of CH₄ or CO₂ adsorption rate incorporates the absolute adsorption amount (n_{abs}). The relationship between n_{abs} and GSE is:

$$n_{\text{abs}} = \frac{\text{GSE}}{1 - \frac{\rho_b}{\rho_a}} \quad (2)$$

where ρ_a and ρ_b are adsorbed phase density and bulk density of adsorbate, respectively, g/cm³. According to previous studies [50], ρ_a of adsorbate is always deemed as a pseudo-liquid state. Therefore, ρ_a of CH₄ and CO₂ were 0.421 g/cm³ and 1.227 g/cm³, respectively [51,52].

2.6. Gas Diffusivity Modelling

Compared to the unipore model, the bidisperse model can well represent the gas adsorption rate behavior in coal pores [53,54]. Therefore, the simplified bidisperse model was chosen to study the gas adsorption rate according to the study of Pan et al. [32]. The bidisperse model consists of a fast macropore diffusion stage and a slow micropore diffusion stage.

The first/fast stage occurs at the beginning of the experiment and can be expressed by:

$$\frac{M_a}{M_{a\infty}} = 1 - \frac{6}{\pi^2} \sum_{n=1}^{\infty} \frac{1}{n^2} \exp\left(-\frac{D_a n^2 \pi^2 t}{R_a^2}\right) \quad (3)$$

where M_a is the total capacity of CH₄ or CO₂ adsorbed in macropore at t , mmol/g; R_a is the macropore radius, m; D_a is the effective diffusivity at macro scale, m²/s; D_a/R_a^2 is the macropore apparent diffusion coefficients, s⁻¹.

The slow stage can be expressed by:

$$\frac{M_i}{M_{i\infty}} = 1 - \frac{6}{\pi^2} \sum_{n=1}^{\infty} \frac{1}{n^2} \exp\left(-\frac{D_i n^2 \pi^2 t}{R_i^2}\right) \quad (4)$$

where M_i is the total capacity of CH₄ or CO₂ adsorbed in micropore at t , mmol/g; R_i is the micropore radius, m; D_i is the effective diffusivity at micro scale, m²/s; D_i/R_i^2 is the micropore apparent diffusion coefficients, s⁻¹.

Combined with Equations (3) and (4), the whole diffusion-adsorption process uptake is given as:

$$\frac{M_t}{M_{\infty}} = \frac{M_a + M_i}{M_{a\infty} + M_{i\infty}} = \beta \frac{M_a}{M_{a\infty}} + (1 - \beta) \frac{M_i}{M_{i\infty}} \quad (5)$$

where β is defined as the ratio of macropore adsorption to the total adsorption [30]. Thus, according to Equation (5), the parameters D_a/R_a^2 , D_i/R_i^2 , and β can be estimated by using nonlinear curve fitting.

3. Results and Discussions

3.1. Gas Diffusivity and Bidisperse Modelling

Figure 3 displays the experimental curves of CH₄ and CO₂ adsorption with time t . Take the case of sample SSP16, the repetitive experiments of CH₄ adsorption with time t , shown in Figure 4, indicates good reproducibility of the diffusion-adsorption measurements. Typically, for both vitrinite- and inertinite-rich coals, the adsorption rate curves of CH₄ and CO₂ display fast adsorption within the initial 1000 s and then gradually approaches the equilibrium state. The bidisperse model exhibits a good fitting with the experimental data of CH₄ and CO₂ adsorption rate. The bidisperse model fitting parameters of gas diffusivity of the coals pre- and post-SFE are listed in Tables 2 and 3, respectively. The correlation coefficients R^2 for all samples were over 0.98, thus implying that the bidisperse pore-diffusion model can well represent CH₄ or CO₂ diffusion behaviors in all samples. Within the whole experimental pressure range, the magnitude orders of D_a/R_a^2 (10^{-3} – 10^{-2}) and D_i/R_i^2 (10^{-5} – 10^{-4}) values of CH₄ and CO₂ apparent diffusion coefficients have a good agreement with the findings by Pan et al. [32] and Cui et al. [54]. Under similar equilibrium pressure, the slope of adsorption rate against time t of CO₂ was higher than that of CH₄ (Figure 3). It is found from Tables 2 and 3 that the pore apparent diffusion coefficients of CO₂ was one order of magnitude larger than that of CH₄ on the same coal sample. The reasons may be related to the molecular kinetics diameter, adsorption interaction between adsorbate and adsorbent, and adsorption heat, which have been addressed in previous studies [54,55].

As presented in Tables 2 and 3, the alterations in values of D_a/R_a^2 and D_i/R_i^2 of CH₄ and CO₂ show that the gas diffusion-adsorption rates of vitrinite- and inertinite-rich coals present different responses to SFE. For vitrinite-rich coals, SFE caused an increase in macropore diffusion coefficients of CH₄ (D_a/R_a^2 increased by 12.19–65.34%), but induced a decline in micropore effective diffusion coefficients of CH₄ (D_i/R_i^2 decreased by 8.75–17.79%). However, the reverse trend was found for the change in pore diffusion coefficients of CO₂ due to SFE, which owned a decrease of 28.95–52.77% and an increase of 17.32–29.80% for D_a/R_a^2 and D_i/R_i^2 , respectively. For inertinite-rich coals after SFE, both the macro- and micropore diffusivity of CH₄ increase. In terms of pore diffusion coefficients of CO₂, the D_a/R_a^2 and D_i/R_i^2 values are 1.25–1.40 times and 0.84–0.95 times, respectively, compared to the original samples. The aforementioned results indicate that macro- and micropore diffusivity of CH₄ and CO₂ vary due to SFE but differ in inertinite-rich coals and vitrinite-rich coals. This phenomenon implies that maceral composition played a dominate role in the change of gas adsorption kinetic behaviors due to SCCO₂ interaction. Moreover, the impact of SFE on pore diffusion was more evident for CO₂ than for CH₄.

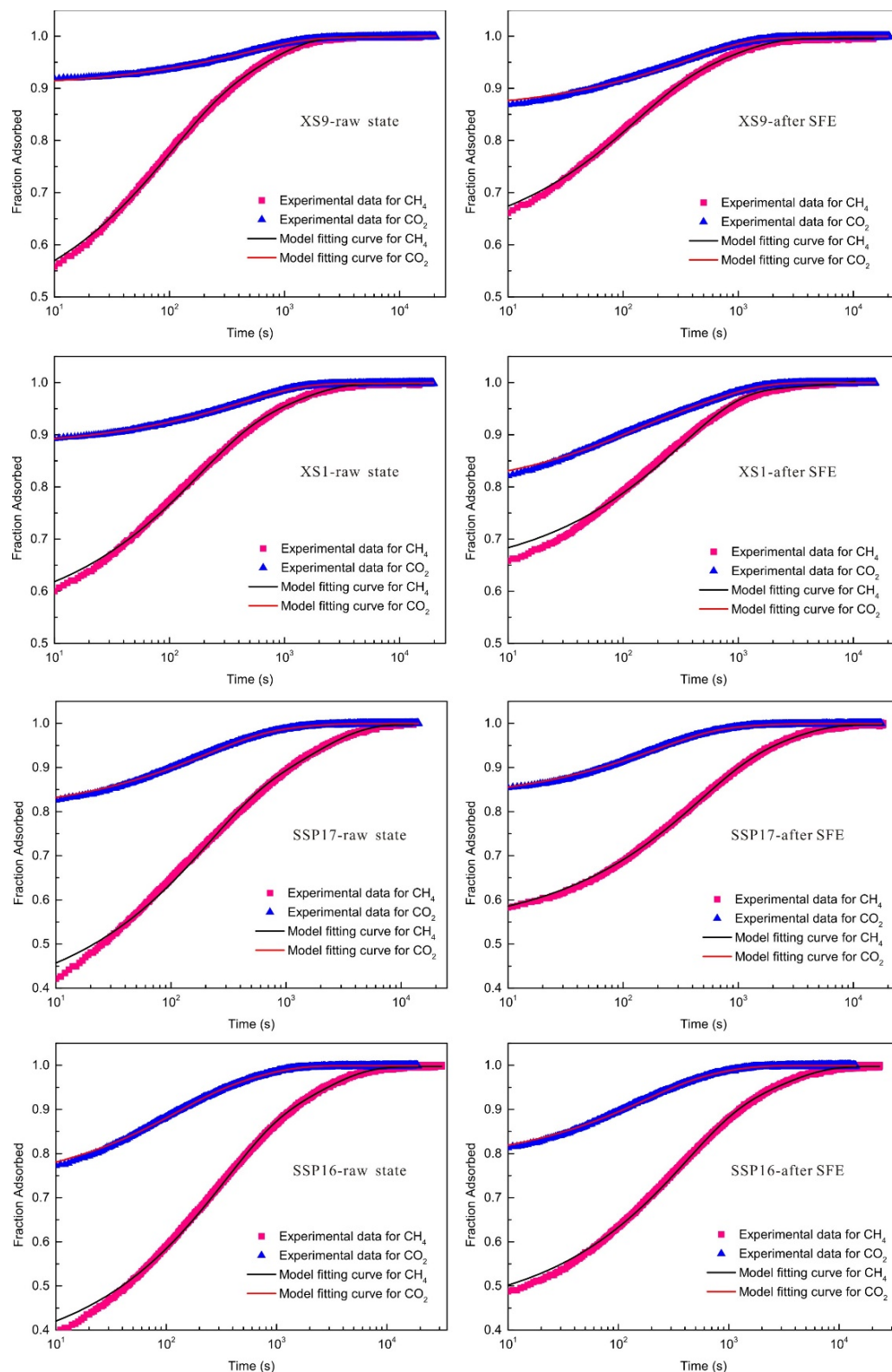


Figure 3. Experimental and fitting curves of CH₄ and CO₂ adsorption rate in samples.

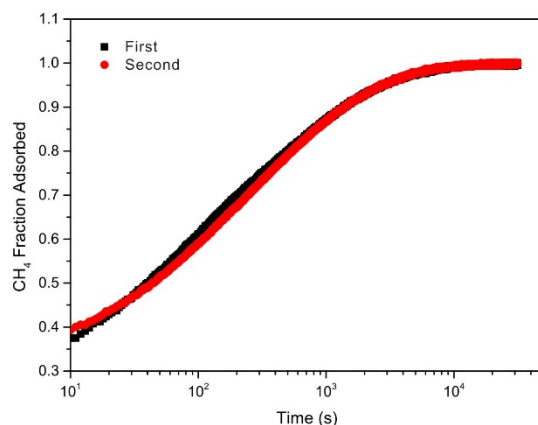


Figure 4. Reproducibility of CH₄ diffusion–adsorption results for SSP16 sample.

Table 2. Statistical results of CH₄ diffusion rate.

Sample Number	State	D_a/R_a^2 (s ⁻¹)	D_i/R_i^2 (s ⁻¹)	β	R^2
XS9	before	4.039×10^{-3}	2.124×10^{-4}	0.636	0.992
	after	6.678×10^{-3}	1.746×10^{-4}	0.716	0.986
XS1	before	4.595×10^{-3}	1.600×10^{-4}	0.676	0.989
	after	5.155×10^{-3}	1.460×10^{-4}	0.668	0.983
SSP17	before	2.190×10^{-3}	6.896×10^{-5}	0.617	0.985
	after	2.546×10^{-3}	7.024×10^{-5}	0.635	0.995
SSP16	before	3.468×10^{-3}	5.653×10^{-5}	0.583	0.984
	after	5.662×10^{-3}	6.444×10^{-5}	0.603	0.985

Table 3. Statistical results of CO₂ diffusion rate.

Sample Number	State	D_a/R_a^2 (s ⁻¹)	D_i/R_i^2 (s ⁻¹)	β	R^2
XS9	before	3.800×10^{-2}	1.349×10^{-4}	0.902	0.992
	after	2.700×10^{-2}	1.751×10^{-4}	0.857	0.989
XS1	before	3.600×10^{-2}	1.611×10^{-4}	0.874	0.995
	after	1.700×10^{-2}	1.890×10^{-4}	0.826	0.991
SSP17	before	2.400×10^{-2}	2.994×10^{-4}	0.822	0.989
	after	3.000×10^{-2}	2.521×10^{-4}	0.805	0.990
SSP16	before	1.500×10^{-2}	2.981×10^{-4}	0.765	0.986
	after	2.100×10^{-2}	2.826×10^{-4}	0.790	0.989

3.2. Influencing Mechanism of SFE on Gas Diffusion

For bidisperse diffusion, as described by Cui et al. [54] and Wei et al. [56], the gas diffusion in coal is mainly controlled by micropore surface diffusion and macro/mesopore diffusion. Many previous studies have shown that pore properties and surface functional groups have a significant impact on gas diffusion–adsorption behaviors [57–60]. The studies of Liu et al. [61] reported that mesopore volume determined the effective diffusion coefficient of CH₄. Wang et al. [39] found that micropore diffusion coefficient was proportional to micropore surface area and was mainly controlled by surface diffusion. Therefore, the variation in the pore structure of inertinite- and vitrinite-rich coals after SCCO₂ interaction should be concerned. Additionally, various kinds of functional groups exist on the coal surface. Numerous studies revealed that the oxygen-containing functional groups showed a great impact on gas adsorption behavior [62]. Thus, the variations in oxygen-containing functional group contents after exposure to SCCO₂ would affect gas diffusion and adsorption in coals. In the present work, the pore parameters and surface

oxygen-containing species distribution before and after SFE were analyzed to account for the possible influencing mechanisms of SFE on gas diffusion.

The PV and SSA of macro/mesopore and micropore are listed in Table 4. SFE increases PV and SSA at macro/mesopore scale of both vitrinite- and inertinite-rich coals (Table 4). SCCO₂ interaction enhances the micropore development of vitrinite-rich coals, while degrading the microporosity of inertinite-rich coals (Table 4). The impact of SFE on pore parameters can be attributed to the physical and chemical reaction, such as coal matrix swelling and extraction effect between SCCO₂ fluid and coal [20,23,25,63]. The distinction between microporosity of the vitrinite- and inertinite-rich coals pre- and post-SFE may be related to the differences in the chemical structure of maceral composition [26], which need further studies. The various SCCO₂-caused changes in pore parameters illustrate the critical roles of maceral type in SCCO₂-coal interaction. Owing to the increased macro/mesopore volume in post-SCCO₂ samples, the macropore diffusivity of CH₄ and CO₂ improved except for the macropore diffusivity of CO₂ in vitrinite-rich coals. However, as shown in Tables 2–4, the varying trend between micropore apparent diffusion coefficients and micropore surface area in the post-SCCO₂ samples was different. For example, the micropore surface area of the inertinite-rich coals decreased while the micropore diffusion coefficients of CH₄ increased. A similar phenomenon can be found in vitrinite-rich coals. This illustrates that the alterations in pore parameters between original and post-CO₂ samples are inadequate to account for the impact of SFE on CH₄ and CO₂ diffusion.

Table 4. Summary of PV and SSA of micro- and macro/mesopore in samples pre- and post-SFE.

Sample Number	State	Meso- and Macropore		Micropore	
		SSA (m ² /g)	PV (10 ⁻³ cm ³ /g)	SSA (m ² /g)	PV (cm ³ /g)
XS9	before	1.372	7.011	133.99	0.0537
	after	1.391	7.297	135.95	0.0545
XS1	before	1.317	6.711	130.23	0.0522
	after	1.615	7.606	130.79	0.0524
SSP17	before	1.207	5.239	129.29	0.0518
	after	1.409	5.536	126.21	0.0506
SSP16	before	1.157	6.372	111.58	0.0447
	after	1.384	7.075	105.61	0.0423

Taking the case of the XS1 sample, Figure 5 depicts the curve-resolved fitting of the XPS C (1s) spectrum with a binding energy between 280 eV and 292 eV. In our study, the functional groups from C (1s) resolving are deconvoluted into C-C/C-H (284.8 eV), C-O (286.3 ± 0.2 eV), and C=O (287.5 ± 0.2 eV) according to previous studies [64,65]. The fitting results of C content, O oxygen content, and different surface functional groups, pre- and post-SFE, are displayed in Table 5. The functional groups of vitrinite-coals and inertinite-rich coals showed different responses to the reaction with SCCO₂. For the post-SCCO₂ vitrinite-rich coals, the C content and C-C/C-H group concentration showed a minor decrease, but the amount of both organic O, C-O, and C=O species increased. However, the opposite trend was recorded for the inertinite-rich coals after SCCO₂ interaction. An evident reduction in C-O and C=O species was found, whereas an increase in C-C/C-H species was recorded (Table 5). The variations in surface functional groups of coals show that SFE made a change in the surface chemistry property, thereby altering diffusion behaviors of CH₄ and CO₂. Hitherto, the mechanisms of chemical interaction of SCCO₂ with oxygen-containing species have still been ambiguous.

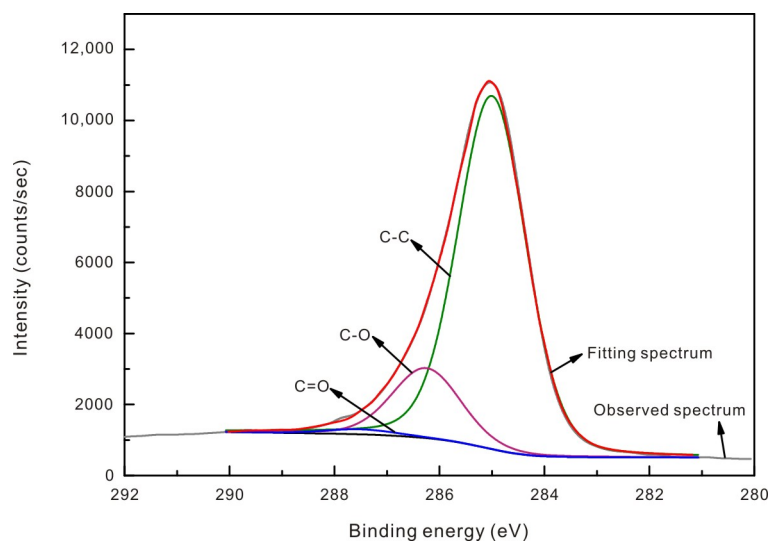


Figure 5. Example of the curve-resolved fitting of XPS C (1s) for the XS1 sample.

Table 5. Surface carbon and organic oxygen content and relative abundance of functional groups.

Sample	State	Surface Composition (%)		Functional Groups (%)		
		C	Organic O	C-C/C-H	C-O	C=O
XS9	before	81.58	4.26	85.12	14.88	0.00
	after	81.33	4.33	84.16	15.84	0.00
XS1	before	80.74	4.33	79.61	20.39	0.00
	after	80.37	4.58	78.95	21.05	0.00
SSP17	before	84.79	5.28	86.88	13.12	0.00
	after	87.81	4.98	88.57	11.43	0.00
SSP16	before	69.42	6.57	80.64	18.36	1.00
	after	72.58	6.04	83.15	16.14	0.70

According to previous studies, the mechanisms are associated with the physical and chemical adsorption of CO₂ on coals. The O atoms of oxygen-containing species own high electronegativity. It favors CO₂ adsorption owing to an inductive effect, which makes CO₂ stably physisorbed on coal surfaces [58]. The work of Huang et al. [66] showed that oxygen-containing species enhanced CO₂ adsorption capacity by hydrogen bonds, which induces CO₂ chemisorbed on coal surfaces. These may decrease the amounts of carbon-oxygen species [67]. Moreover, the mechanism relates to the extraction of SCCO₂ fluid. SCCO₂ fluid can mobilize polycyclic aromatic hydrocarbons, aliphatic species, and low-molecular-weight compounds [11], which can be testified by our XPS results with the decline in C-C/C-H groups of vitrinite-rich coals due to SFE (Table 5). Both the physical-chemical adsorption and extraction effects can contribute to the decrease of different functional group species. As shown in Table 5, the extraction interaction of SCCO₂ with vitrinite-rich coals may be strong, which causes the decrease of C-C/C-H species and the relative enrichment of carbon-oxygen species. Compared to the vitrinite-rich coals, more oxygen-containing functional groups exist in the inertinite-rich coal surface, which provides more preferential polar sites for CO₂ sorption. The chemical interaction of SCCO₂ with carbon-oxygen species may be superior to the extraction effect, thus leading to an apparent reduction of C-O and C=O species concentrations of the inertinite-rich coals.

Many studies show that oxygen-containing species can weaken Van der Waals interactions between CH₄ and pore surface on one hand and block pore on the other [68,69], thus decreasing CH₄ adsorption capacity of coals. However, hydrogen bonds, high electronegativity, and electrostatic contribution between oxygen-containing species and CO₂ favor CO₂ adsorption [23,29,62,70]. The works of Prinz et al. [71] showed that the oxygen-containing

groups might accommodate micropores (0.5–0.8 nm) of the coals with $R_{o,max}$ above 1.5%. Thus, the redistribution of oxygen-containing species due to $SCCO_2$ interaction would alter gas diffusion and adsorption behaviors on the coal micropore surface. According to the aforementioned analyses, in combination with data in Table 5, it can be inferred that the increasing oxygen-containing species of vitrinite-rich coals decreases the diffusivity of CH_4 on the micropore surface but enhances CO_2 diffusivity. Although SFE increases the micropore SSA of the vitrinite-rich coals, the effect of oxygen-containing species may be superior to the micropore surface area. Thus, the net result is that $SCCO_2$ interaction leads to decreasing micropore diffusion coefficients of CH_4 but increasing CO_2 micropore diffusion coefficients in the vitrinite-rich coals. Furthermore, the migration of low-molecular-weight compounds and aliphatic species extracted by $SCCO_2$ fluid may affect CH_4 and CO_2 diffusion. The extracted organic species in vitrinite-rich coals may migrate into the macro/mesopores [72]. These organic species can enhance the adsorption potential of CH_4 on coals by increasing adsorption heat [73] but hinder pore entrance for CO_2 diffusion [72]. This may be another reason for the decrease in the diffusion rate of CO_2 and the increase in the diffusion rate of CH_4 in the macro/mesopore of the vitrinite-rich coals. For the inertinite-rich coals after SFE, the reduction in both oxygen-containing species and micropore SSA improve the diffusivity of CH_4 in micropore but weaken CO_2 diffusion in micropores. Moreover, coal matrix swelling may occur when CO_2 adsorbs on oxygen-containing species and micropore surface, which may compress micropore space and transform some micropores into mesopores. As a result, the concomitant reduction in micropore surface area and rise in mesopore volume occur. This phenomenon may improve macropore diffusion coefficients but degrade micropore diffusion coefficients of CO_2 in inertinite-rich coals. These results obtained from this study indicate that whether vitrinite- or inertinite-rich coals, the comprehensive effect of pore parameters and in coals due to $SCCO_2$ exposure contributes to the different changes in both CH_4 and CO_2 diffusion properties. However, the role of maceral composition in the change of pore and surface functional groups after SFE is different.

3.3. Implications of Maceral Composition for CO_2 Sequestration

In our present study, CO_2 exhibits a higher pore diffusivity than CH_4 , which manifests the viability of improving CH_4 recovery by CO_2 displacement [74]. As discussed in a previous analysis, pore parameters and surface functional groups related to maceral composition after $SCCO_2$ interaction are of great significance in CH_4 and CO_2 diffusion. Thus, the influence of maceral composition on gas diffusivities after $SCCO_2$ -interaction can not be ignored during CO_2 -ECBM implementation. For the vitrinite-rich coals after $SCCO_2$ interaction, the micropore diffusion coefficients of CH_4 decrease while those of CO_2 increase, which benefits displacement of CH_4 by CO_2 injection. However, the reduction in macropore diffusion coefficients of CO_2 may slow CO_2 diffusion and weaken CO_2 displacement efficiency. Thus, for coal reservoirs with high content of vitrinite, it is necessary to consider how to improve the transport and diffusion capacity of CO_2 in macro/mesopores during the CO_2 injection process. In terms of the inertinite-rich coals after $SCCO_2$ exposure, $SCCO_2$ exposure obviously decreases diffusivities of CO_2 in micropores, but increases diffusivities of CH_4 in micropores. This result may impair CH_4 recovery by CO_2 injection; therefore, for coal reservoirs with high content of inertinite, it is required to consider how to mitigate the adverse influence of SFE on micropore structure and surface chemistry. Generally, the detrimental effect of SFE on CH_4 recovery and CO_2 diffusion in coals with different maceral compositions should be fully evaluated for target CO_2 -ECBM projects.

4. Conclusions

This study mainly addressed the influence of supercritical CO_2 fluid on CH_4 and CO_2 diffusion in vitrinite-rich coals and inertinite-rich coals. The main conclusions are included below.

- (1) The bidisperse-pore diffusion model can well analyze CH₄ and CO₂ diffusion behaviors in all samples. In comparison with the original inertinite-rich coal samples, SFE increases the pore diffusivity of CH₄ at both macro- and microscale and enhances the macropore diffusivity of CO₂, but weakens the micropore diffusion rate of CO₂. For the vitrinite-rich coal samples after SCCO₂ interaction, an increase in macropore diffusivity and a decrease in micropore diffusivity of CH₄ are recorded, while the opposite trend is noticed for macro- and micropore diffusion rate of CO₂. The different SCCO₂-induced changes in CH₄ and CO₂ diffusion in the vitrinite- and inertinite-rich coals illustrate the importance of maceral composition in SCCO₂-coal interaction.
- (2) Pore parameter analysis shows that SFE increases macro/mesopore volume of all samples and enlarges micropore SSA of vitrinite-rich coals but degrades that of inertinite-rich coals. The XPS results show that SCCO₂ interaction causes the increase of oxygen-containing species of vitrinite-rich coals, while it results in a decrease of oxygen-containing species of the inertinite-rich coals. The comprehensive result of pore parameters and functional group distribution in different maceral compositions accounting for the roles of SFE on CH₄ and CO₂ diffusion. As a result, different adverse effects may occur after the interaction of SCCO₂ with vitrinite- and inertinite-rich coals. Therefore, the impact of SFE on CH₄ and CO₂ diffusion in coals with different maceral compositions should be fully evaluated in practical CO₂-ECBM projects.

Author Contributions: Conceptualization and methodology, W.L. (Wei Li) and W.L. (Weili Lin); validation, H.L., W.L. (Wei Li) and X.S.; formal analysis, W.L. (Weili Lin); investigation, Z.W.; resources, Z.W.; data curation, W.L. (Weili Lin); writing—original draft preparation, W.L. (Wei Li); writing—review and editing, W.L. (Wei Li); visualization, H.L. and X.S.; supervision, Z.W.; project administration, Z.W.; funding acquisition, Z.W. All authors have read and agreed to the published version of the manuscript.

Funding: This research was funded by the Science Foundation of PetroChina Company Limited, grant number 2021DQ0107-1.

Institutional Review Board Statement: Not applicable.

Informed Consent Statement: Not applicable.

Data Availability Statement: Not applicable.

Acknowledgments: This work is supported by the National Natural Science Foundation of China (No. 41902176), Outstanding Youth Fund of (No. YQ2021D005), University Nursing Program for Young Scholars with Creative Talents in Heilongjiang Province (No. UNPYSCT-2020145), Heilongjiang Postdoctoral Financial Assistance (No. LBH-Z19121), and Youth Science Fund of Northeast Petroleum University (No. 2018QNL-24).

Conflicts of Interest: The authors declare no conflict of interest.

References

1. Blunden, J.; Arndt, D.S. State of the Climate in 2016. *Bull. Am. Meteorol. Soc.* **2017**, *98*, S1–S280. [[CrossRef](#)]
2. Chabangu, N.; Beck, B.; Hicks, N.; Botha, G.; Viljoen, J.; Davids, S.; Cloete, M. The investigation of CO₂ storage potential in the Zululand Basin in South Africa. *Energy Procedia* **2014**, *63*, 2789–2799. [[CrossRef](#)]
3. Zhao, W.Z.; Su, X.B.; Xia, D.P.; Hou, S.H.; Wang, Q.; Zhou, Y.X. Enhanced coalbed methane recovery by the modification of coal reservoir under the supercritical CO₂ extraction and anaerobic digestion. *Energy* **2022**, *259*, 124914. [[CrossRef](#)]
4. Li, Y.; Pan, S.Q.; Ning, S.Z.; Shao, L.Y.; Jing, Z.H.; Wang, Z.S. Coal measure metallogeny: Metallogenic system and implication for resource and environment. *Sci. China Earth Sci.* **2022**, *65*, 1211–1228. [[CrossRef](#)]
5. White, C.M.; Smith, D.H.; Jones, K.L.; Goodman, L.A.; Jikich, S.A.; LaCount, R.B.; DuBose, S.B.; Ozdemir, E.; Morsi, B.I.; Schroeder, K.T. Sequestration of carbon dioxide in coal with enhanced coalbed methane recovery: A review. *Energy Fuels* **2005**, *19*, 659–724. [[CrossRef](#)]
6. Orr, F.M., Jr. Onshore Geologic Storage of CO₂. *Science* **2009**, *325*, 1656–1658. [[CrossRef](#)]
7. Holliday, D.W.; Williams, G.M.; Holloway, S.; Savage, D.; Bannon, M.P. *A Preliminary Feasibility Study for the Underground Disposal of Carbon Dioxide in the UK*; British Geological Survey: Nottingham, UK, 1991; p. 24.

8. Heidaryan, E.; Hatami, T.; Rahimi, M.; Moghadasi, J. Viscosity of pure carbon dioxide at supercritical region: Measurement and correlation approach. *J. Supercrit. Fluids* **2011**, *56*, 144–151. [[CrossRef](#)]
9. Jarrahan, A.; Heidaryan, E. A novel correlation approach to estimate thermal conductivity of pure carbon dioxide in the supercritical region. *J. Supercrit. Fluids* **2012**, *64*, 39–45. [[CrossRef](#)]
10. Heidaryan, E.; Jarrahan, A. Modified Redlich-Kwong equation of state for supercritical carbon dioxide. *J. Supercrit. Fluids* **2013**, *81*, 92–98. [[CrossRef](#)]
11. Kolak, J.J.; Burruss, R.C. The use of solvent extractions and solubility theory to discern hydrocarbon associations in coal, with application to the coal-supercritical CO₂ system. *Org. Geochem.* **2014**, *73*, 56–69. [[CrossRef](#)]
12. Ren, J.G.; Niu, Q.H.; Wang, Z.Z.; Wang, W.; Yuan, W.; Weng, H.B.; Sun, H.W.; Li, Y.C.; Du, Z.G. CO₂ adsorption/desorption, induced deformation behavior, and permeability characteristics of different rank coals: Application for CO₂-Enhanced coalbed methane recovery. *Energy Fuels* **2022**, *36*, 5709–5722. [[CrossRef](#)]
13. Liu, X.Q.; Li, M.J.; Zhang, C.H.; Fang, R.H.; Zhong, N.N.; Xue, Y.; Zhou, Y.; Jiang, W.D.; Chen, X.Y. Mechanistic insight into the optimal recovery efficiency of CBM in sub-bituminous coal: Through molecular simulation. *Fuel* **2020**, *266*, 117137. [[CrossRef](#)]
14. Sampath, K.H.S.M.; Sin, I.; Perera, M.S.A.; Matthai, S.K.; Ranjith, P.G.; Li, D.Y. Effect of supercritical-CO₂ interaction time on the alterations in coal pore structure. *J. Nat. Gas Sci. Eng.* **2020**, *76*, 103214. [[CrossRef](#)]
15. Chen, K.; Liu, X.F.; Wang, L.K.; Song, D.Z.; Nie, B.S.; Yang, T. Influence of sequestered supercritical CO₂ treatment on the pore size distribution of coal across the rank range. *Fuel* **2021**, *306*, 121708. [[CrossRef](#)]
16. Gao, S.S.; Jia, L.L.; Zhou, Q.J.; Cheng, H.F.; Wang, Y. Microscopic pore structure changes in coal induced by a CO₂-H₂O reaction system. *J. Pet. Sci. Eng.* **2022**, *208*, 109361. [[CrossRef](#)]
17. Zhang, G.L.; Ranjith, P.G.; Li, Z.S.; Vongsvivut, J.; Gao, M.Z. Application of synchrotron ATR-FTIR microspectroscopy for chemical characterization of bituminous coals treated with supercritical CO₂. *Fuel* **2021**, *296*, 120639. [[CrossRef](#)]
18. Zhang, G.L.; Ranjith, P.G.; Lyu, Q. Direct evidence of CO₂ softening effects on coal using nanoindentation. *Energy* **2022**, *254*, 124221. [[CrossRef](#)]
19. Mirzaei, M.; Hall, P.J.; Jirandehi, H.F. Study of structural change in Wyodak coal in high-pressure CO₂ by small angle neutron scattering. *J. Mater. Sci.* **2010**, *45*, 5271–5281. [[CrossRef](#)]
20. Liu, S.Q.; Sang, S.X.; Ma, J.S.; Wang, T.; Du, Y.; Fang, H.H. Effects of supercritical CO₂ on micropores in bituminous and anthracite coal. *Fuel* **2019**, *242*, 96–108. [[CrossRef](#)]
21. Zhang, H.; Hu, Z.C.; Xu, Y.; Fu, X.; Li, W.; Zhang, D.F. Impacts of long-term exposure to supercritical carbon dioxide on physicochemical properties and adsorption and desorption capabilities of moisture-equilibrated coals. *Energy Fuels* **2021**, *35*, 12270–12287. [[CrossRef](#)]
22. Zhang, D.F.; Li, C.; Zhang, M.; Lun, Z.M.; Jia, S.Q.; Luo, C.J.; Jiang, W.P. Influences of dynamic entrainer-blended supercritical CO₂ fluid exposure on high-pressure methane adsorption on coals. *J. Nat. Gas Sci. Eng.* **2019**, *66*, 180–191. [[CrossRef](#)]
23. Mastalerz, M.; Drobniak, A.; Walker, R.; Morse, D. Coal lithotypes before and after saturation with CO₂: Insights from micro- and mesoporosity, fluidity, and functional group distribution. *Int. J. Coal Geol.* **2010**, *83*, 467–474. [[CrossRef](#)]
24. Sha, F.; Deng, B.Z.; Yin, G.Z.; Zhang, D.M.; Li, M.H.; Liu, P.; Liu, C. Kinetic behavior of heterogeneous sorption deformation on coal: Effect of maceral/micro-lithotype distribution. *Int. J. Coal Geol.* **2019**, *216*, 103324. [[CrossRef](#)]
25. Mastalerz, M.; Drobniak, A.; Rupp, J. Meso- and micropore characteristics of coal lithotypes: Implications for CO₂ adsorption. *Energy Fuels* **2008**, *22*, 4049–4061. [[CrossRef](#)]
26. Cao, X.Y.; Mastalerz, M.; Chappell, M.A.; Miller, L.F.; Li, Y.; Mao, J.D. Chemical structures of coal lithotypes before and after CO₂ adsorption as investigated by advanced solid-state ¹³C nuclear magnetic resonance spectroscopy. *Int. J. Coal Geol.* **2011**, *88*, 67–74. [[CrossRef](#)]
27. Karacan, C.O.; Mitchell, G.D. Behavior and effect of different coal microlithotypes during gas transport for carbon dioxide sequestration into coal seams. *Int. J. Coal Geol.* **2003**, *53*, 201–217. [[CrossRef](#)]
28. Maphala, T.; Wagner, N.J. Effects of CO₂ storage in coal on coal properties. *Energy Procedia* **2012**, *23*, 426–438. [[CrossRef](#)]
29. Mavhengere, P.; Maphala, T.; Wagner, N. Physical and structural effects of carbon dioxide storage on vitrinite-rich coal particles under subcritical and supercritical conditions. *Int. J. Coal Geol.* **2015**, *150–151*, 1–6. [[CrossRef](#)]
30. Naveen, P.; Asif, M.; Ojha, K.; Panigrahi, D.C.; Vuthaluru, H.B. Sorption kinetics of CH₄ and CO₂ diffusion in coal theoretical and experimental study. *Energy Fuels* **2017**, *31*, 6825–6837. [[CrossRef](#)]
31. Song, Y.; Quan, F.K.; Yuan, J.H. Diffusion of guest molecules in coal: Insights from simulation. *Fuel* **2022**, *323*, 124295.
32. Pan, J.Z.; Connell, L.D.; Camilleri, M.; Connelly, L. Effects of matrix moisture on gas diffusion and flow in coal. *Fuel* **2003**, *82*, 1219–1229. [[CrossRef](#)]
33. Bai, J.J.; Kang, Y.L.; Chen, M.J.; Liang, L.; You, L.J.; Li, X.C. Investigation of multi-gas transport behavior in shales via a pressure pulse method. *Chem. Eng. J.* **2019**, *360*, 1667–1677. [[CrossRef](#)]
34. Liu, L.F.; Wang, Y.H.; Aryana, S.A. Insights into scale translation of methane transport in nanopores. *J. Nat. Gas Sci. Eng.* **2021**, *96*, 104220. [[CrossRef](#)]
35. Liu, L.F.; Nieto-Draghi, C.; Lachet, V.; Heidaryan, E.; Aryana, S. A. Bridging confined phase behavior of CH₄-CO₂ binary systems across scales. *J. Supercrit. Fluids* **2022**, *189*, 105713. [[CrossRef](#)]
36. Keshavarz, A.; Sakurovs, R.; Grigore, M.; Sayyafzadeh, M. Effect of maceral composition and coal rank on gas diffusion in Australian coals. *Int. J. Coal Geol.* **2017**, *173*, 65–75. [[CrossRef](#)]

37. Guang, W.F.; Liu, X.Q.; Zhang, Z.Y.; Luo, P. Effects of sub- and supercritical CO₂ on coal diffusivity and surface thermodynamics. *Energy Fuels* **2022**, *36*, 3737–3748. [[CrossRef](#)]
38. Goodman, A.L.; Favors, R.N.; Larsen, J.W. Argonne coal structure rearrangement caused by sorption of CO₂. *Energy Fuels* **2006**, *20*, 2537–2543. [[CrossRef](#)]
39. Wang, Q.Q.; Li, W.; Zhang, D.F.; Wang, H.H.; Jiang, W.P.; Zhu, L.; Tao, J.; Huo, P.L.; Zhang, J. Influence of CO₂ exposure on adsorption kinetics of methane and CO₂ on coals. *J. Nat. Gas Sci. Eng.* **2016**, *34*, 811–822. [[CrossRef](#)]
40. Li, W.; Liu, H.F.; Song, X.X. Multifractal analysis of Hg pore size distributions of tectonically deformed coals. *Int. J. Coal Geol.* **2015**, *144–145*, 138–152. [[CrossRef](#)]
41. Unsworth, J.F.; Fowler, C.S.; Jones, L.F. Moisture in coal 2. Maceral effects on pore structure. *Fuel* **1989**, *68*, 18–26. [[CrossRef](#)]
42. Li, W.; Liu, H.F.; Song, X.X. Influence of fluid exposure on surface chemistry and pore-fracture morphology of various rank coals: Implications for methane recovery and CO₂ storage. *Energy Fuels* **2017**, *31*, 12552–12569. [[CrossRef](#)]
43. Busch, A.; Gensterblum, Y.; Krooss, B.M.; Littke, R. Methane and carbon dioxide adsorption-diffusion experiments on coal: Upscaling and modeling. *Int. J. Coal Geol.* **2004**, *60*, 151–168. [[CrossRef](#)]
44. Wang, H.B.; Li, T.; Zou, Q.L.; Cheng, Z.H.; Yang, Z.K. Influences of path control effects on characteristics of gas migration in a coal reservoir. *Fuel* **2020**, *267*, 117212. [[CrossRef](#)]
45. Goodman, A.L.; Busch, A.; Duffy, G.J.; Fitzgerald, J.E.; Gasem, K.A.M.; Gensterblum, Y.; Krooss, B.M.; Levy, J.; Ozdemir, E.; Pan, Z.; et al. An inter-laboratory comparison of CO₂ isotherms measured on Argonne premium coal samples. *Energy Fuels* **2004**, *18*, 1175–1182. [[CrossRef](#)]
46. Sing, K.S.W.; Everett, D.H.; Haul, R.A.W.; Moscou, L.; Pierotti, R.A.; Rouquerol, J.; Siemieniewska, T. Reporting physisorption data for gas/solid systems with special reference to the determination of surface area and porosity. *Pure Appl. Chem.* **1985**, *57*, 603–619. [[CrossRef](#)]
47. Weitzsacker, C.L.; Gardella, J.A., Jr. Quantitative electron spectroscopic analysis of the surface chemistry of bituminous coals. *Energy Fuels* **1996**, *10*, 141–148. [[CrossRef](#)]
48. Wanger, W.; Span, R. Special equations of state for methane, argon, and nitrogen for the temperature range from 270 to 350 K at pressures up to 30 MPa. *Int. J. Thermophys.* **1993**, *14*, 699–725.
49. Span, R.; Wanger, W. A New equation of state for carbon dioxide covering the fluid region from the triple-point temperature to 1100 K at pressures up to 800 MPa. *J. Phys. Chem. Ref. Data* **1996**, *25*, 1509–1596. [[CrossRef](#)]
50. Zhang, D.F.; Cui, Y.J.; Liu, B.; Li, S.G.; Song, W.L.; Lin, W.G. Supercritical pure methane and CO₂ adsorption on various rank coals of China: Experiments and modeling. *Energy Fuels* **2011**, *25*, 1891–1899. [[CrossRef](#)]
51. Harpalani, S.; Prusty, B.K.; Dutta, P. Methane/CO₂ sorption modeling for coalbed methane production and CO₂ sequestration. *Energy Fuels* **2006**, *20*, 1591–1599. [[CrossRef](#)]
52. Siemons, N.; Busch, A. Measurement and interpretation of supercritical CO₂ sorption on various coals. *Int. J. Coal Geol.* **2007**, *69*, 229–242. [[CrossRef](#)]
53. Clarkson, C.R.; Bustin, R.M. The effect of pore structure and gas pressure upon the transport properties of coal: A laboratory and modeling study. 2. Adsorption rate modeling. *Fuel* **1999**, *78*, 1345–1362. [[CrossRef](#)]
54. Cui, X.J.; Bustin, R.M.; Dipple, G. Selective transport of CO₂, CH₄, and N₂ in coals: Insights from modeling of experimental gas adsorption data. *Fuel* **2004**, *83*, 293–303. [[CrossRef](#)]
55. Sakurovs, R.; Day, S.; Weir, S. Relationships between the critical properties of gases and their high pressure sorption behavior on coals. *Energy Fuels* **2010**, *24*, 1781–1787. [[CrossRef](#)]
56. Wei, X.R.; Wand, G.X.; Massarotto, P.; Golding, S.D.; Rudolph, V. Numerical simulation of multicomponent gas diffusion and flow in coals for CO₂ enhanced coalbed methane recovery. *Chem. Eng. Sci.* **2007**, *62*, 4193–4203. [[CrossRef](#)]
57. Gensterblum, Y.; Busch, A.; Krooss, B.M. Molecular concept and experimental evidence of competitive adsorption of H₂O, CO₂ and CH₄ on organic material. *Fuel* **2014**, *115*, 581–588. [[CrossRef](#)]
58. Liu, Y.Y.; Wilcox, J. Molecular simulation studies of CO₂ adsorption by carbon model compounds for carbon capture and sequestration applications. *Environ. Sci. Technol.* **2013**, *47*, 95–101. [[CrossRef](#)] [[PubMed](#)]
59. Bai, J.J.; Kang, Y.L.; Chen, M.J.; Chen, Z.X.; You, L.J.; Li, X.C.; Chen, G. Impact of surface chemistry and pore structure on water vapor adsorption behavior in gas shale. *Chem. Eng. J.* **2020**, *402*, 126238. [[CrossRef](#)]
60. Li, Y.; Yang, J.H.; Pan, Z.J.; Tong, W.S. Nanoscale pore structure and mechanical property analysis of coal: An insight combining AFM and SEM images. *Fuel* **2020**, *260*, 116352. [[CrossRef](#)]
61. Liu, H.H.; Mou, J.H.; Cheng, Y.P. Impact of pore structure on gas adsorption and diffusion dynamics for long-flame coal. *J. Nat. Gas Sci. Eng.* **2015**, *22*, 203–213. [[CrossRef](#)]
62. Liu, Y.Y.; Wilcox, J. Molecular simulation of CO₂ adsorption in micro- and mesoporous carbons with surface heterogeneity. *Int. J. Coal Geol.* **2012**, *104*, 83–95. [[CrossRef](#)]
63. Liu, C.J.; Sang, S.X.; Zhang, K.; Song, F.; Wang, H.W.; Fan, X.F. Effects of temperature and pressure on pore morphology of different rank coals: Implications for CO₂ geological storage. *J. CO₂ Util.* **2019**, *34*, 343–352. [[CrossRef](#)]
64. Kelemen, S.R.; Afeworki, M.; Gorbaty, M.L. Characterization of organically bound oxygen forms in lignites, peats, and pyrolyzed peats by X-ray photoelectron spectroscopy (XPS) and solid-state ¹³C NMR methods. *Energy Fuels* **2002**, *16*, 1450–1462. [[CrossRef](#)]
65. Kelemen, S.R.; Kwiatek, P.J. Quantification of organic oxygen species on the surface of fresh and reacted argonne premium coal. *Energy Fuels* **1995**, *9*, 841–848. [[CrossRef](#)]

66. Huang, X.; Chu, W.; Sun, W.J.; Jiang, C.F.; Feng, Y.Y.; Xue, Y. Investigation of oxygen-containing group promotion effect on CO₂-coal interaction by density functional theory. *Appl. Surf. Sci.* **2014**, *299*, 162–169. [[CrossRef](#)]
67. Mirzaeian, M.; Hall, P.J. The interactions of coal with CO₂ and its effects on coal structure. *Energy Fuels* **2006**, *20*, 2022–2027. [[CrossRef](#)]
68. Hao, S.X.; Wen, J.; Yu, X.P.; Chu, W. Effect of the surface oxygen groups on methane adsorption on coals. *Appl. Surf. Sci.* **2013**, *264*, 433–442. [[CrossRef](#)]
69. Cuervo, M.R.; Asedegbega-Nieto, E.; Díaz, E.; Ordóñez, S.; Vega, A.; Dongil, A.B.; Rodríguez-Ramos, I. Modification of the adsorption properties of high surface area graphites by oxygen functional groups. *Carbon* **2008**, *46*, 2096–2106. [[CrossRef](#)]
70. Lu, X.Q.; Jin, D.L.; Wei, S.X.; Zhang, M.M.; Zhu, Q.; Shi, X.F.; Deng, Z.G.; Guo, W.Y.; Shen, W.Z. Competitive adsorption of a binary CO₂-CH₄ mixture in nanoporous carbons: Effects of edge-functionalization. *Nanoscale* **2015**, *7*, 1002–1012. [[CrossRef](#)]
71. Prinz, D.; Pyckhout-Hintzen, W.; Littke, R. Development of the meso- and macroporous structure of coals with rank as analysed with small angle neutron scattering and adsorption experiments. *Fuel* **2004**, *83*, 547–556. [[CrossRef](#)]
72. Bae, J.-S.; Bhatia, S.K.; Rudolph, V.; Massarotto, P. Pore accessibility of methane and carbon dioxide in coals. *Energy Fuels* **2009**, *23*, 3319–3327. [[CrossRef](#)]
73. Zhou, F.B.; Liu, S.Q.; Pang, Y.Q.; Li, J.L.; Xin, H.H. Effects of coal functional groups on adsorption microheat of coal bed methane. *Energy Fuels* **2015**, *29*, 1550–1557. [[CrossRef](#)]
74. Li, Y.; Wang, Y.B.; Wang, J.; Pan, Z.J. Variation in permeability during CO₂-CH₄ displacement in coal seams: Part 1—Experimental insights. *Fuel* **2020**, *263*, 116666. [[CrossRef](#)]

Disclaimer/Publisher’s Note: The statements, opinions and data contained in all publications are solely those of the individual author(s) and contributor(s) and not of MDPI and/or the editor(s). MDPI and/or the editor(s) disclaim responsibility for any injury to people or property resulting from any ideas, methods, instructions or products referred to in the content.